Advanced Energy Conversion Materials
https://ojs.wiserpub.com/index.php/AECM/

UNIVERSAL WISER PUBLISHER

Research Article

Novel $CaMoO_4$@GO Nanocomposite: Synthesis, Characterization, and Investigation Its Photocatalytic Properties

Seyed Mostafa Hosseinpour Mashkani

Young Researchers and Elites Club, Arak Branch, Islamic Azad University, Arak, Iran
E-mail: Hosseinpour.sm@gmail.com

Received: 24 March 2020; **Revised:** 15 June 2020; **Accepted:** 16 June 2020

Abstract: The current study aims to synthesize and characterize Calcium Molybdate-Graphene Oxide ($CaMoO_4$@GO) nanocomposite under ultrasonic irradiation. Primarily, degradation of Methylene blue (MB) under ultraviolet-visible spectroscopy (Uv-Vis) light was investigated to measure the photocatalytic properties of the as-synthesized $CaMoO_4$@GO nanocomposite. In addition, various graphene oxide concentrations were applied to investigate its impact on the optical and photodegradation properties of calcium molybdate. X-ray diffraction (XRD), scanning electron microscopy (SEM), and spectra energy dispersive analysis of X-ray (EDS) were used to characterize $CaMoO_4$@GO nanocomposite. DRS results demonstrated that GO influenced significantly the optical properties of $CaMoO_4$ as much as band gap of $CaMoO_4$@GO nanocomposite shows a redshift in comparison with pure $CaMoO_4$. Consequently, photocatalytic results demonstrated that adding GO causes to increase photodegradation of MB form 65% ($CaMoO_4$) to 89% ($CaMoO_4$@GO).

***Keywords*:** $CaMoO_4$@GO nanocomposite, ultrasonic method, photocatalytic, redshift

1. Introduction

In the third millennium, the human lifestyle has undergone huge changes due to the industrial revolution. As a result, various kinds of pollution including water, air, soil, noise, etc. have been emerging. Water pollution, as one of the main pollutions, damaged human life and the environment. Inorganic and organic dyes known as the main source of water pollution have been extensively used in different industries such as paper, plastics, textiles, and rubber industries. Over their advantages, they have many disadvantages including high toxicity, high environmental stability, and potentially irresolvable. There are many traditional techniques for treating dyes in wastewaters which are ineffective and costly [1]. With introducing nanotechnology into the wastewater purification technologies, novel photocatalytic semiconductor nanomaterials have been developed. In the past decade, there has been a considerable attention to the semiconductor nanoparticles because of their unique physical properties which make them suitable for different applications [2-9]. Besides, their ideal band gap makes them appropriate photocatalytic candidates for degradation of environmental pollutants such as detergents, pesticides, dyes, and volatile organic compounds under UV/Vis light [10-16]. $CaMoO_4$ in which Ca atom exhibits eight-fold oxygen coordination and the Mo atom forms a MoO_4^{2-} tetrahedron, has gained lots of attention due to its high chemical stability. In addition, it's interesting luminescence properties which result of energy transfer from host lattice to the dopant ions ($AMoO_4$ (A = Ca, Sr, Ba)) [17, 18] leading to its

DOI: https://doi.org/10.37256/aecm.122020333

wide application in white light-emitting diodes, displays, and devices in photochemical fields [19-22]. On the other hand, $CaMoO_4$ has potential applications in various areas including phosphor microparticles and acousto-optic filters, catalyst, microwave applications, solid-state lasers, phosphor microparticles, energy storage, the blue phosphor in fluorescent lighting devices and Microwave Amplification by Stimulated Emission of Radiation (MASER) materials, in medical applications as scintillator, humidity sensors, Li-ion batteries, fluorescent lamps, photoluminescence, photocatalytic, nano-pigment, etc [23-26]. Various techniques have been used for synthesizing $CaMoO_4$ such as the Czochralski method [27], coprecipitation [28], combustion [29], and conventional solid-state reaction [30]. Due to the fascinating luminescence properties of $CaMoO_4$, in the current study, a ultrasonic method was applied to synthesize $CaMoO_4$ nanoparticles to investigate its photocatalytic properties. In order to enhance the photocatalytic properties of the as-synthesized $CaMoO_4$ nanoparticles, graphene oxide was used to make a hybrid nanocomposite ($CaMoO_4$@GO). Besides, methylene blue (MB) was used to measure the photocatalytic ability of $CaMoO_4$ nanoparticles and its nanocomposite ($CaMoO_4$@GO) under Uv-Vis light.

2. Characterization

X-ray diffraction (XRD) patterns were recorded by a Philips-X'PertPro, X-ray diffractometer using Ni-filtered Cu Kα radiation at the scan range of $10 < 2\theta < 80$. Scanning electron microscopy (SEM) images were obtained on LEO-1455VP equipped with an energy dispersive X-ray spectroscopy. The energy dispersive spectrometry (EDS) analysis was studied by XL30, Philips microscope. Ultrasonic irradiation was performed using a high-intensity ultrasonic probe (Sonicator 3000; Bandeline, MS 72, Germany, Tihorn, 20 kHz, 60 Wcm^{-2}) immersed directly in the reaction solution.

3. Synthesis of $CaMoO_4$ nanoparticles

All the chemicals used were of analytical grade and without any further purification. The stoichiometric ratio of $(NH_4)_6Mo_7O_{24}\cdot 4H_2O$ and $Ca(NO_3)_2\cdot 6H_2O$ were dissolved in 30 ml of distilled water, separately. Then, after heating $Ca(NO_3)_2\cdot 6H_2O$ solution up to 50 °C for 10 min, $(NH_4)_6Mo_7O_{24}\cdot 4H_2O$ solution was added dropwise to it. Eventually, the final mixed solution was ultrasonicated at 100 W for 30 min. After ultrasonication, the mixture was cooled to room temperature naturally and the obtained white precipitate was collected by filtration, washed with absolute ethanol and distilled water several times, and was dried in vacuum at 50 °C for 120 min.

4. Synthesis of $CaMoO_4$@GO nanocomposites

In order to synthesize semiconductor nanocomposite ($CaMoO_4$@GO), various molar ratios of graphene oxide were mixed with $CaMoO_4$ nanoparticles under ultrasonic waves (100 W) for 20 min. After irradiation, the precipitates were washed, centrifuged, and dried in vacuum at 60 °C for 2 h.

5. Photocatalytic experiments

Photodegradation of Methylene blue (MB) under Uv-Vis light was performed in the presence of $CaMoO_4$ nanoparticles and its nanocomposite ($CaMoO_4$@GO) to investigate their photocatalytic properties and subsequently the impact of GO on the photocatalytic properties of $CaMoO_4$ nanoparticles. Photodegradation experiments were run in the presence of $CaMoO_4$/$CaMoO_4$@GO (20 mg) and MB solution (150 mL of 5 mg/L solution) under Uv-Vis light. Before exposing to the light, the mixture solution of dye and nanoparticles was kept in darkness (30 min) in order to establish adsorption-desorption equilibrium between the dye molecules and nanoparticle surface. After 30 min, it was exposed to the 500 W Xe lamp while 10 mL of mixture solution was taken out (each 15 min), centrifuged, and their absorbances were recorded. The MB degradation percentage was calculated as:

$$\text{Degradation rate (\%)} = 100\ (A_0 - A)/A_0$$

where A_0 and A are the absorbance value of the solution at A_0 and A min, respectively.

6. Results and discussion

Figure 1a-c shows the XRD patterns of $CaMoO_4$ nanoparticles, GO, and $CaMoO_4$@GO nanocomposites, respectively. Figure 1a indicates the formation of tetragonal phase of $CaMoO_4$ with calculated cell parameters a = b = 5.2260 *Å* and c = 11.4300 *Å*, space group of I41/a, and JCPDS No. 29-0351. Based on the XRD pattern of GO (Figure 1b), the peak at 2θ = 12.5° is assigned to the GO (002) [31]. Moreover, the XRD spectrum of $CaMoO_4$@GO nanocomposites (Figure 1c) demonstrates tetragonal phase of $CaMoO_4$ (space group I41/a and JCPDS No. 29-0351) along with the peak at 2θ = 12.5°, related to the GO. Based on the Debye Scherrer Eq. (1) and XRD data, the crystallite diameter (*Dc*) of $CaMoO_4$ nanoparticles and $CaMoO_4$@GO nanocomposites are measured to be 23 nm and 19.5 nm, respectively:

$$D_c = K\lambda/\beta cos\theta \tag{1}$$

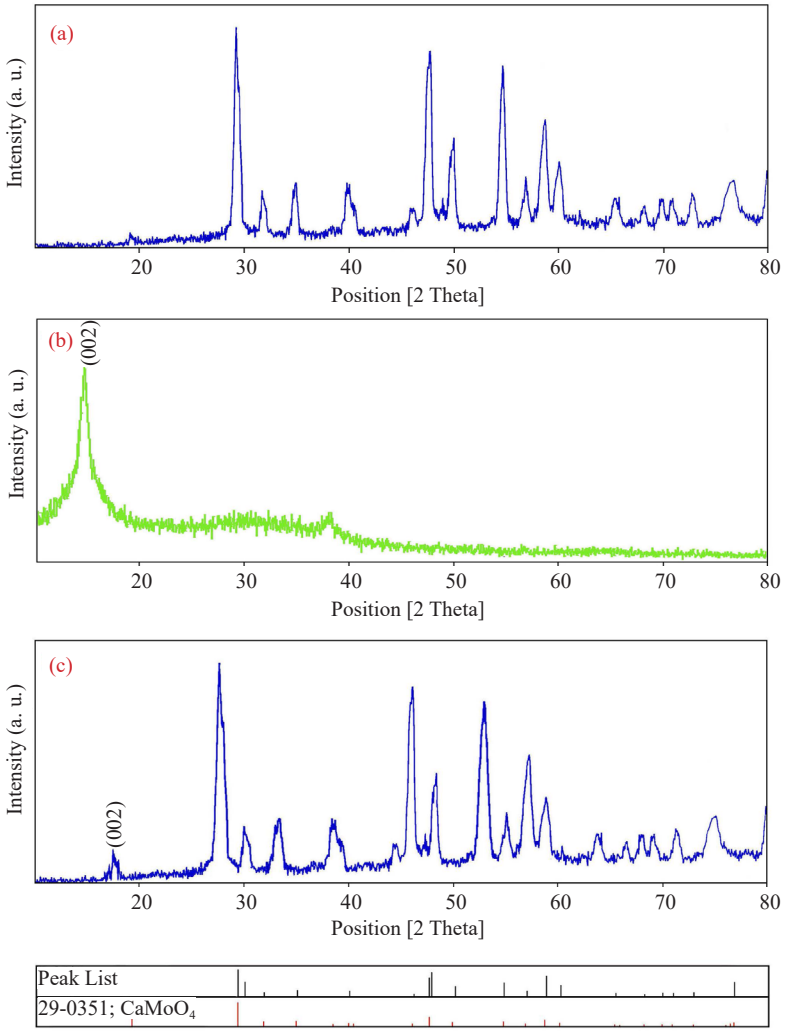

Figure 1. XRD patterns of (a) $CaMoO_4$ nanoparticles (b) GO (c) $CaMoO_4$@GO nanocomposites

where β is the breadth of the observed diffraction line at its half intensity maximum, K is the so-called shape factor, which usually takes a value of about 0.9, and λ is the wavelength of X-ray source used in XRD. Doping the GO into the $CaMoO_4$ nanoparticles causes the crystal size to decrease form 23 nm to 19.5 nm. In other words, XRD characteristic peaks of $CaMoO_4$ in nanocomposite are broader than those in pure $CaMoO_4$ nanoparticles which could be related to the increasing the nucleation sites due to the increase in the functional groups as a result of doping GO [32, 33]. Energy-dispersive X-ray spectroscopy (EDS) was applied to further examine the purity of $CaMoO_4$ nanoparticles, as shown in Figure 2. EDS analysis shows that $CaMoO_4$ consists of only Ca, Mo, and O elements. Scanning electron microscopy was used to investigate the morphology of GO, $CaMoO_4$ nanoparticles, and $CaMoO_4$@GO nanocomposites, as shown in Figure 3a-c, respectively. SEM images of $CaMoO_4$ nanoparticle and GO show that they mainly consists of spherical nanoparticles and sheet structure, respectively. In addition, $CaMoO_4$@GO nanocomposites SEM images show that $CaMoO_4$@GO composed of sheets and nanoparticles. Tauc's relationship ($\alpha = \alpha 0\ (h\nu\text{-}Eg)\ n/h\nu$) has been using to measure the electronic bandgap of semiconductors. Where α (α = 2.303A/t) is the absorption coefficient, h and ν are Planck's constant and the photon energy, respectively. In addition, $\alpha 0$ is the constants, E_g is the optical band gap of the material, and n depends on the type of electronic transition and can be any value between $1/2$ and 3. The band gaps of $CaMoO_4$, GO, and $CaMoO_4$@GO nanocomposites, with various GO concentrations, could be calculated through the extrapolating the linear portion of the plots of $(\alpha h\nu)^{1/2}$ against $h\nu$ to the energy axis, as shown in Figure 4. The bandgaps of $CaMoO_4$ and $CaMoO_4$@GO nanocomposites (GO = 0.02 to 0.1 g corresponding to the samples 1-5) are 3.3, 3.29, 3.15, 3.14, 3.1, and 3 eV, respectively. Doping the GO into the $CaMoO_4$ nanoparticles, narrows its bandgap energy and shift absorption edge towards higher wavelengths due to an increase of surface charge in presence of GO which is thanks to the unpaired π electrons of GO surface. As a result, absorption ability of $CaMoO_4$@GO nanocomposites was enhanced in the visible light region. Methylene blue (MB), an organic pollutant, was selected in order to assess the photocatalytic properties of $CaMoO_4$ and $CaMoO_4$@GO nanocomposites under Uv-Vis light, as shown in Figure 5. Based on Figure 5, in the presence of $CaMoO_4$ nanoparticles, MB was degraded 65%. On the other hand, doping GO into the $CaMoO_4$ nanoparticles causes increase degradation by 89% after 90 min (Table 1). The enhancing photodegradation mechanism of MB in the presence of $CaMoO_4$@GO nanocomposites can be explain as follows [34, 35]. At first, light induces MB dye molecules to the higher energy level in which a photoexcited e^- from VB of $CaMoO_4$ jumps to its CB follow by jumping into the GO. GO, as an electron acceptor, acts as a suppressive agent which suppresses the recombination of charge carriers due to its twodimensional π-conjugation structure. Afterwards, electrons from GO react with environmental oxygen to create superoxide radicals ($O^{\bullet}_2^-$) and then holes in the VB react with H_2O_2 to create hydroxyl radicals (OH°). Finally, intermediates, water, and CO_2 produce due to the oxidizing MB by OH° and $O^{\bullet}_2^-$ species. By comparing to other published works, the current study shows maximum photocatalyst yield in lower degradation time, due to the presence of GO [36, 37].

Table 1. Degradation yield of MB in the presence of $CaMoO_4$ nanoparticles and $CaMoO_4$@GO nanocomposites (sample 1-5)

Sample no	MB degradation (%)	Band gap (eV)
$CaMoO_4$	65	3.3
1	69	3.29
2	75	3.15
3	78	3.14
4	82	3.1
5	89	3

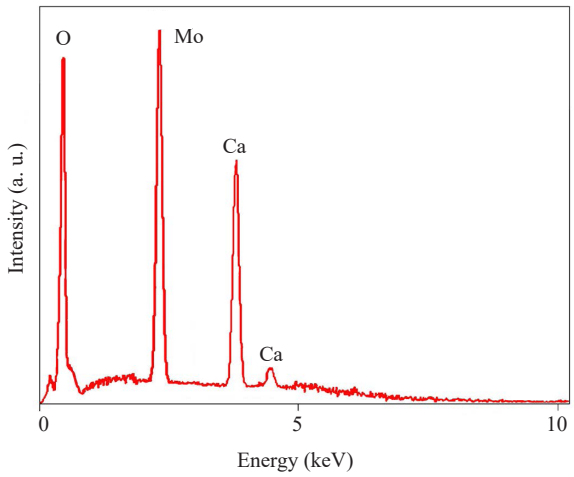

Figure 2. EDS pattern of $CaMoO_4$ nanoparticles

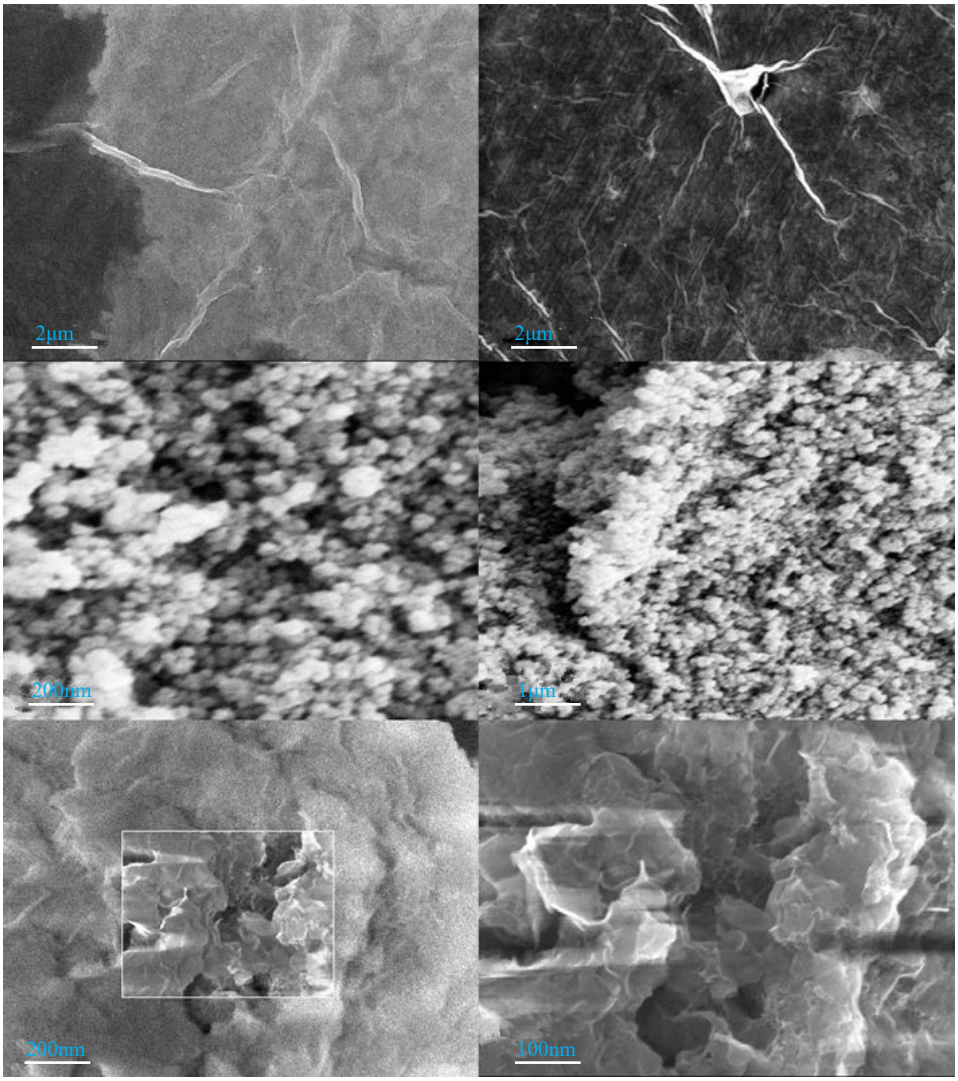

Figure 3. SEM images of (a) GO (b) $CaMoO_4$ nanoparticles (c) $CaMoO_4$@GO nanocomposites

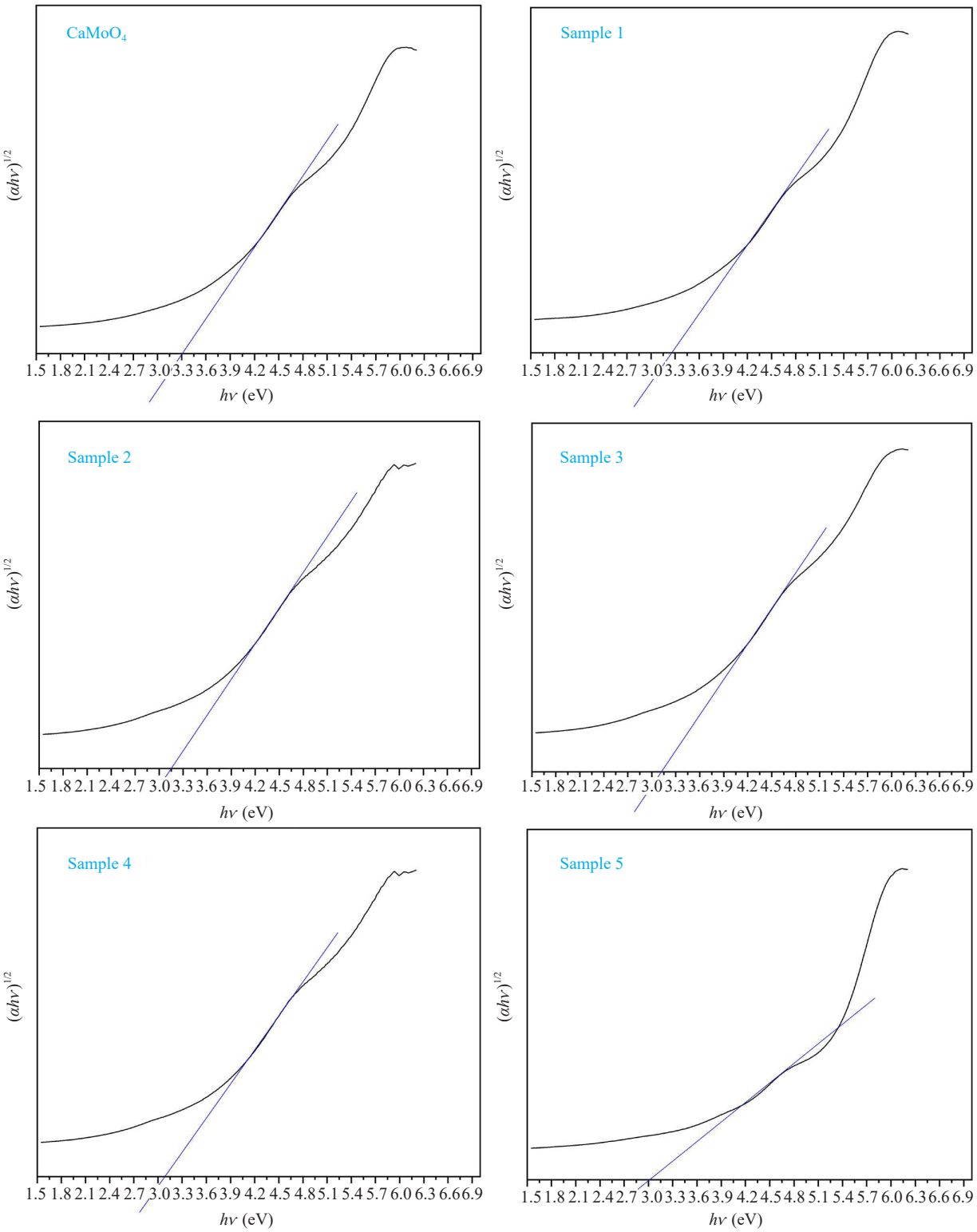

Figure 4. UV-Vis patterns of $CaMoO_4$ and $CaMoO_4$@GO nanocomposites

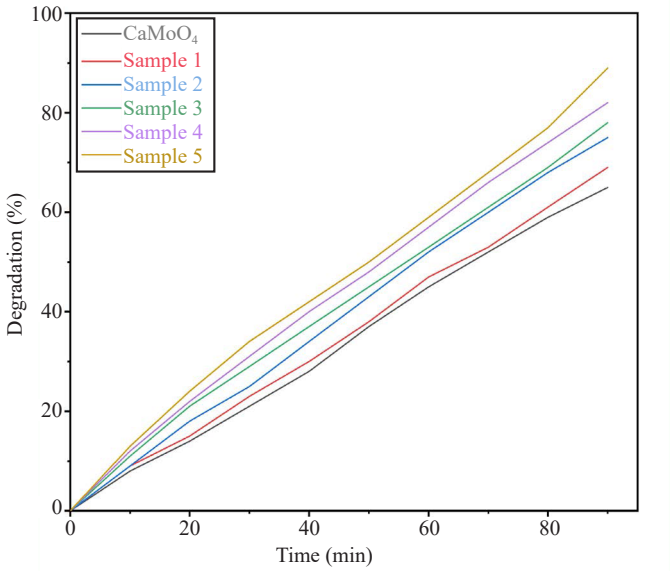

Figure 5. Photodegradation of MB in the presence of $CaMoO_4$ nanoparticles and $CaMoO_4$@GO nanocomposites (sample 1-5)

7. Conclusions

In summary, $CaMoO_4$ and its composite ($CaMoO_4$@GO) were synthesized under the ultrasonic wave. The impacts of various graphene oxide concentrations on the optical and photocatalytic properties of $CaMoO_4$ were investigated. Degradation of methylene blue (MB) was examined to evaluate the photocatalytic properties of $CaMoO_4$ and $CaMoO_4$@GO. Photodegradation results revealed that increasing the GO concentration causes to increase in the degradation percentage of MB due to the increase visible light absorption by $CaMoO_4$@GO nanocomposites.

Acknowledgment

The authors are grateful to the council of the University of Arak for providing financial support to undertake this work and Padideh Noavaran Nano Bonyan Company, Iran.

Conflict of interest

Authors declare that they do not have any conflict of interest.

References

[1] Evgenidou E, Konstantinou I, Fytianos K, Poulios I, Albanis T. Photocatalytic oxidation of methyl parathion over TiO_2 and ZnO suspensions. *Catal Today*. 2007; 124: 156-162.
[2] Tu S, Zhang Y, Reshak AH, Auluck S, Ye L, Han X, et al. Ferroelectric polarization promoted bulk charge separation for highly efficient CO_2 photoreduction of $SrBi_4T_{i4}O_{15}$. *Nano Energy*. 2019; 56: 840-850.
[3] Reshak AH. Active photocatalytic water splitting solar-to-hydrogen energy conversion: Chalcogenide photocatalyst Ba_2ZnSe_3 under visible irradiation. *Applied Catalysis B: Environmental*. 2018; 221: 17-26.
[4] Reshak AH. Sulfide oxide XZnSO (X = Ca or Sr) as novel active photocatalytic water splitting solar-to-hydrogen energy conversion. *Applied Catalysis B: Environmental*. 2018; 225: 273-283.
[5] Reshak AH. A novel photocatalytic water splitting solar-to-hydrogen energy conversion: Non-centro-symmetric borate $CsZn_2B_3O_7$ photocatalyst. *Journal of Alloys and Compounds*. 2018; 741: 1258-1268.

[6] Huang H, Reshak AH, Auluck S, Jin S, Tian N, Guo Y, et al. Visible-light-responsive sillén-structured mixed-cationic $CdBiO_2Br$ nanosheets: layer structure design promoting charge separation and pxygen activation reactions. *The Journal of Physical Chemistry C*. 2018; 122(5): 2661-2672.
[7] Reshak AH. Novel photocatalytic water splitting solar-to-hydrogen energy conversion: $CdLa_2S_4$ and $CdLa_2Se_4$ ternary semiconductor compounds. *Physical Chemistry Chemical Physics.* 2018; 20: 8848-8858.
[8] Reshak AH. Chairlike and boatlike graphane: Active photocatalytic water splitting solar-to-hydrogen energy conversion under UV irradiation. *Physical Chemistry Chemical Physics*. 2018; 122: 8076-8081.
[9] Reshak AH. AA- and ABA-stacked carbon nitride (C_3N_4): novel photocatalytic water splitting solar-to-hydrogen energy conversion. *Physical Chemistry Chemical Physics*. 2018; 20: 22972-22979.
[10] Hosseinpour-Mashkani SM, Maddahfar M, Sadeghinia A, Ramezani M. $PbSe@PbSO_4$ nanoparticles: sonochemical synthesis and characterization and its photocatalytic degradation of methylene blue. *Journal of Materials Science: Materials in Electronics*. 2015; 26: 3352-3356.
[11] Gholami A, Nikkhah-Amirabad T, Maddahfar M. Investigation of photovoltaic properties of silver-doped $ZnTiO_3$ nanoparticles. *Journal of Materials Science: Materials in Electronics*. 2017; 28: 15327-15332.
[12] Gholami A, Maddahfar M. Synthesis and characterization of barium molybdate nanostructures with the aid of amino acids and investigation of its photocatalytic degradation of methyl orange. *Journal of Materials Science: Materials in Electronics*. 2016; 27: 6773-6778.
[13] Hosseinpour-Mashkani SM, Maddahfar M, Sobhani-Nasab A. Precipitation synthesis, characterization, morphological control, and photocatalyst application of $ZnWO_4$ nanoparticles. *Journal of Electronic Materials*. 2016; 45: 3612-3620.
[14] Gholami A, Maddahfar M. Synthesis and characterization of novel samarium-doped $CuAl_2O_4$ and its photocatalytic performance through the modified sol-gel method. *Journal of Materials Science: Materials in Electronics*. 2016; 27: 3341-3346.
[15] Hosseinpour-Mashkani SM, Maddahfar M, Sobhani-Nasab A. Novel silver-doped $CdMoO_4$: synthesis, characterization, and its photocatalytic performance for methyl orange degradation through the sonochemical method. *Journal of Materials Science: Materials in Electronics*. 2016; 27: 474-480.
[16] Maddahfar M, Ramezani M, Sadeghi M, Sobhani-Nasab A. $NiAl_2O_4$ nanoparticles: synthesis and characterization through modify sol-gel method and its photocatalyst application. *Journal of Materials Science: Materials in Electronics*. 2015; 26: 7745-7750.
[17] Cornu L, Jubera V, Demourgues A, Salek G, Gaudon M. Luminescence properties and pigment properties of A-doped (Zn, Mg) MoO_4 triclinic oxides (with A = Co, Ni, Cu or Mn). *Ceramics International*. 2017; 43: 13377-13387.
[18] Cho WS, Yashima M, Kakihana M, Kudo A, Sakata T, Yoshimura M. Active electrochemical dissolution of molybdenum and application for room-temperature synthesis of crystallized luminescent calcium molybdate film. *Journal of the American Ceramic Society*. 1997; 8: 765-769.
[19] Musikhin AE, Naumov VN, Bespyatov MA, Shlegel VN. Heat capacity and thermodynamic functions of $CaMoO_4$ at low temperatures. *Journal of Alloys and Compounds*. 2016; 655: 165-171.
[20] Sarantopoulou E, Raptis C, Ves S, Christofilos D. Temperature and pressure dependence of Raman-active phonons of $CaMoO_4$: an anharmonicity study. *Journal of Physics: Condensed Matter*. 2002; 14: 8925-8938.
[21] Han Y, Wang L, Wang D, Liang D, Wang S, Lu G, et al. Lanthanide ions-doped calcium molybdate pie-like microstructures: Synthesis, structure characterization, and luminescent properties. *Journal of Alloys and Compounds*. 2017; 695: 3018-3023.
[22] Laguna M, Nuñez NO, Becerro AI, Ocaña M. Morphology control of uniform $CaMoO_4$ microarchitectures and development of white light emitting phosphors by Ln doping (Ln = Dy^{3+}, Eu^{3+}). *Crystal Engineering Communication*. 2017; 19: 1590-1600.
[23] Ponta O, Ciceo-Lucacel R, Vulpoi A, Radu T, Simon V, Simon S. Synthesis and characterisation of nanostructured silica-powellite-HAP composites. *Journal of Materials Science*. 2015; 50: 577-586.
[24] Li X, Fan G, Huang Z. Synthesis and surface thermodynamic functions of $CaMoO_4$ nanocakes. *Entropy*. 2015; 17: 2741-2748.
[25] Bhanvase BA, Kadam VB, Rode TD, Jadhao PR. Sonochemical process for the preparation of novel calcium zinc molybdate nanoparticles. *International Journal of Nanoscience*. 2015; 14: 1550014-1550023.
[26] Kusuma M, Chandrappa GT. Effect of calcination temperature on characteristic properties of $CaMoO_4$ nanoparticles. *Journal of Science: Advanced Materials and Devices*. 2019; 4: 150-157.
[27] Grasser R, Pitt E, Scharmann A, Zimmerer G. Optical properties of $CaWO_4$ and $CaMoO_4$ crystals in the 4 to 25eV

region. *Physica Status Solidi B*. 1975; 69: 359-368.
[28] Paski EF, Blades MW. Ananlysis of inorganic powders by time wavelength resolved luminescence spectroscopy. *Analytical Chemistry*. 1988; 60: 1224-1230.
[29] Yang P, Yao GQ, Lin JH. Photoluminescence and combustion synthesis of $CaMoO_4$ doped with Pb^{2+}. *Inorganic Chemistry Communications*. 2004; 7: 389-391.
[30] Sleight AW. Accurate cell dimensions for ABO_4 molybdates and tungstates. *Structural Science*. 1972; 28: 2899-2902.
[31] Shalaby A, Nihtianova D, Markov P, Staneva A. Structural analysis of reduced graphene oxide by transmission electron microscopy. *Bulgarian Chemical Communications*. 2015; 47: 291-295.
[32] Dreyer DR, Park S, Bielawski CW, Ruoff S. The chemistry of graphene oxide. *Chemical society reviews*. 2010; 39: 228-240.
[33] Abrinaeia F, Kimiagarb S, Zolghadrc S. Hydrothermal synthesis of hematite-GO nanocomposites at different GO contents and potential application in nonlinear optics. *Optical Materials*. 2019; 96: 109285.
[34] Giovannetti R, Rommozzi E, Zannotti M, D'Amato C. Recent advances in graphene based TiO_2 nanocomposites ($GTiO_2N_s$) for photocatalytic degradation of synthetic dyes. *Catalysts*. 2017; 7: 305-339.
[35] Li B, Liu T, Wang Y, Wang Z. ZnO/graphene-oxide nanocomposite with remarkably enhanced visible-light-driven photocatalytic performance. *Journal of colloid and interface science*. 2012; 377: 114-121.
[36] Huerta-Flores AM, Juárez-Ramírez I, Torres-Martínez LM, Carrera-Crespo JE, Gómez-Bustamante T, Sarabia-Ramos O. Synthesis of $AMoO_4$ (A = Ca, Sr, Ba) photocatalysts and their potential application for hydrogen evolution and the degradation of tetracycline in water. *Journal of Photochemistry and Photobiology A: Chemistry*. 2018; 356: 29-37.
[37] Hosseinpour-Mashkani SS, Hosseinpour-Mashkani SS, Sobhani-Nasab A. Synthesis and characterization of rodlike $CaMoO_4$ nanostructure via free surfactant sonochemical route and its photocatalytic application. *Journal of Materials Science: Materials in Electronics*. 2016; 27: 4351-4355.